JGR Earth Surface

RESEARCH ARTICLE
10.1029/2021JF006325

Wintertime Brine Discharge at the Surface of a Cold Polar Glacier and the Unexpected Absence of Associated Seismicity

C. G. Carr[1,2], J. D. Carmichael[2], and E. C. Pettit[3]

[1]University of Alaska Fairbanks, Fairbanks, AK, USA, [2]Los Alamos National Laboratory, Los Alamos, NM, USA, [3]Oregon State University, Corvallis, OR, USA

Key Points:

- Time-lapse photos capture wintertime Blood Falls brine release
- Brine release occurs without evidence for enhanced Rayleigh wave seismicity near the release point
- The Blood Falls crack may open as a series of small fracture events, masked by local seismicity

Supporting Information:

Supporting Information may be found in the online version of this article.

Correspondence to:

C. G. Carr,
cgcarr@lanl.gov

Citation:

Carr, C. G., Carmichael, J. D., & Pettit, E. C. (2022). Wintertime brine discharge at the surface of a cold polar glacier and the unexpected absence of associated seismicity. *Journal of Geophysical Research: Earth Surface*, *127*, e2021JF006325. https://doi.org/10.1029/2021JF006325

Received 24 JUN 2021
Accepted 3 FEB 2022

Author Contributions:

Conceptualization: C. G. Carr, J. D. Carmichael, E. C. Pettit
Data curation: C. G. Carr, E. C. Pettit
Formal analysis: C. G. Carr, J. D. Carmichael, E. C. Pettit
Funding acquisition: E. C. Pettit
Investigation: C. G. Carr, J. D. Carmichael, E. C. Pettit
Methodology: C. G. Carr, J. D. Carmichael, E. C. Pettit
Project Administration: E. C. Pettit
Resources: J. D. Carmichael, E. C. Pettit
Software: C. G. Carr, J. D. Carmichael
Supervision: J. D. Carmichael, E. C. Pettit
Validation: C. G. Carr, J. D. Carmichael

Abstract A subglacial groundwater system beneath Taylor Glacier, Antarctica, discharges hypersaline, iron-rich brine episodically at the glacier surface to create Blood Falls. However, the triggering mechanism for these brine release events is not yet understood. Identifying which fracture processes are observed seismically can help us better characterize the hydrological system at Taylor Glacier, and more generally, provide us with a broader understanding of englacial hydrologic activity in cold glaciers. We document wintertime brine discharge using time-lapse photography. Subfreezing air temperatures during the brine discharge indicate that surface melt-induced hydrofracture is an unlikely trigger for brine release. Further, we analyze local seismic data to test a hypothesis that fracturing generates elevated surface wave energy preceding and/or coinciding with brine release events. Our results show no discernible elevated Rayleigh wave activity prior to or during Blood Falls brine release. Instead, we find a pattern of seismic events dominated by a seasonal signal, with more Rayleigh events occurring in the summer than the winter from the Blood Falls source area. We calculate that the volumetric opening of cracks that would generate Rayleigh waves at our detection limits are of similar size to myriad cracks in glacier ice, lake ice, and frozen sediment in the terminus area. We therefore propose that any fracturing coincident with brine release activity likely consists of a series of smaller opening events that are masked by other seismicity in the local environment.

Plain Language Summary Blood Falls is a reddish feature that forms at the terminus of Taylor Glacier in Antarctica when hypersaline, iron-rich brine flows from sediment under the glacier up through the ice to emerge from cracks at the surface. We used data from a time-lapse camera and nearby seismic sensors to document a brine release. Our images show a brine release event starting in May 2014 (austral winter), and fractures in the glacier surface observed following the event encouraged us to hypothesize that we would detect an increase in Rayleigh waves (a type of seismic wave that can be generated by surface crack opening). However, we do not observe an increase in Rayleigh wave activity prior to or during brine release. When we estimate the average size of the fractures that we detect, we find the size is similar to many types of cracks in the nearby environment (for instance, cracks in the lake ice). We conclude that any Rayleigh wave seismicity that occurred during the Blood Falls brine release must be from a series of crack openings smaller than our detection limit, and that other cracks opening in the nearby environment may mask any signal specific to the Blood Falls release.

1. Introduction

Episodic discharge of subglacially sourced, iron-rich brine at the terminus of Taylor Glacier, Antarctica, forms the feature named Blood Falls (Figure 1). The brine discharges over weeks to months during releases that occur several times per decade, and can occur during any season. Brine deposits have primarily been observed at two subaerial locations: the Blood Falls site at the glacier surface and, less frequently, at a lateral site where brine icings have been observed in the ice-marginal stream bed at the northern terminus margin. Compilations of brine release activity and brine deposit observations include Black (1969), Carr (2021), Keys (1979), and Lawrence (2017). In this paper, we focus on the Blood Falls site; therefore, phrases like "brine discharge" and "brine release event" refer to discharge at the Blood Falls site unless otherwise specified.

An unresolved question is what triggers the episodic brine release. Carmichael et al. (2012) hypothesize that meltwater-driven fracturing during the summer melt season could propagate deep enough into the glacier to trigger brine outflow. However, springtime observations of brine icing superimposed on lake ice (e.g., Black, 1969; Keys, 1979) indirectly suggest that brine releases can occur during the wintertime in the absence of surface

Visualization: C. G. Carr, J. D. Carmichael
Writing – original draft: C. G. Carr
Writing – review & editing: C. G. Carr, J. D. Carmichael, E. C. Pettit

melt. This implies that meltwater-driven fracture cannot explain all brine release events. Cracks in the glacier surface are often observed following a brine release event; these cracks extend tens of meters from the terminus up-glacier and can be on the order of tens of centimeters wide (Figure S1 in Supporting information S1). These cracks observed near Blood Falls suggest that seismic activity could be used to monitor brine release activity. Seismometers are particularly helpful instruments during periods when human observers are not present, or when polar night makes time-lapse photography difficult.

Here, we use time-lapse photography to document a brine release event that began in winter 2014 (Figure 1). Large surface cracks were visible when researchers arrived the following summer field season (2014–2015; Figure S1 in Supporting Information S1). Surface crack opening generates Rayleigh waves, a type of seismic surface wave, including in glacial settings (e.g., Carmichael et al., 2015; Deichmann et al., 2000; Mikesell et al., 2012; Neave & Savage, 1970). Therefore, we test the hypothesis that the opening of Blood Falls-related cracks at the glacier surface generates detectable Rayleigh waves with elevated seismicity (number of seismic events per unit of time) prior to and/or during the brine release activity observed in the time-lapse photos from the winter.

2. Background

2.1. Blood Falls: An Episodically Active Hydrologic Feature at Taylor Glacier

Taylor Glacier is an outlet glacier of the East Antarctic Ice Sheet. The glacier flows into Taylor Valley, where the central portion of the terminus ends in ice-capped Lake Bonney (Figure 2a). Typical ice temperatures are near −17°C in the terminus region (Pettit et al., 2014). The supraglacial component of the hydrologic system is active during the short melt season, typically from late November through mid-January. During this time, most meltwater generated on the glacier either runs off the glacier in large supraglacial melt channels (Johnston et al., 2005) or pools in cryoconite holes (shallow ponds) that refreeze at the glacier surface (Fountain et al., 2004). Pathways for meltwater delivery into the glacier consist of crevasses, which are only present near the ice cliff margins and within the last few hundred meters of the terminus; moulins or similar deep connections to the englacial or subglacial components are absent.

Wintertime discharge events at Blood Falls result in the buildup of a fan-shaped icing deposit that drapes over the proglacial moraine and Lake Bonney ice surface (Black et al., 1965). Icings (also called naled, aufeis, or overflow) form in a variety of environmental settings when subsurface water emerges and refreezes at the ground surface and have been documented at polythermal and cold-based glaciers. At these other glaciers, englacially or subglacially stored meltwater emerges at the ice surface or out of proglacial sediments to produce icings (e.g., Hodgkins et al., 2004; Irvine−Fynn et al., 2011; Skidmore & Sharp, 1999). At Taylor Glacier, summertime discharge events also occur, but do not create the same icings because the brine freezing point is much lower than typical summertime air temperatures. For terms like ‘summertime’, we follow the season definitions of Obryk et al. (2020) wherein the month of October is spring, November–February are summer, March is autumn, and April–September are winter.

Airborne electromagnetic surveys of Taylor Valley reveal several connected groundwater systems (Foley et al., 2016; Mikucki et al., 2015), including the subglacial groundwater system beneath the Taylor terminus. Blood Falls can be considered a groundwater spring and Lake Bonney a terminal lake in this system, with an estimated 1.5 km^3 of brine-saturated sediments extending under the ice for at least 6 km up-glacier from the lake (Mikucki et al., 2015). Ice thickness gradients resulting from highly incised surface channels in the terminus area impose strong hydraulic potential gradients at the glacier bed that route some subglacial flow toward Blood Falls and some toward the central terminus (Badgeley et al., 2017) where subglacial brine discharges directly into proglacial Lake Bonney (Lawrence et al., 2020). Less frequently, brine also discharges through sediment at lateral sites near the glacier margin (Carr, 2021; Chapter 2).

Following the winter 2014 brine release described in this paper, englacially stored brine was sampled in-situ during the following summer field season (Badgeley et al., 2017; Campen et al., 2019; Kowalski et al., 2016; Lyons et al., 2019). The brine can remain liquid despite the cold ice temperatures due to salinity-driven freezing point depression, and presumably also due to latent heat effects. Geochemistry of the brine outflow at Blood Falls further suggests the subglacial brine has been isolated from the atmosphere for an extended time (Mikucki et al., 2009); stratigraphic evidence from drill cores in Taylor Valley suggest possible isolation since the late Miocene-early Pliocene (Elston & Bressler, 1981). Microbial analysis of brine collected from englacial storage

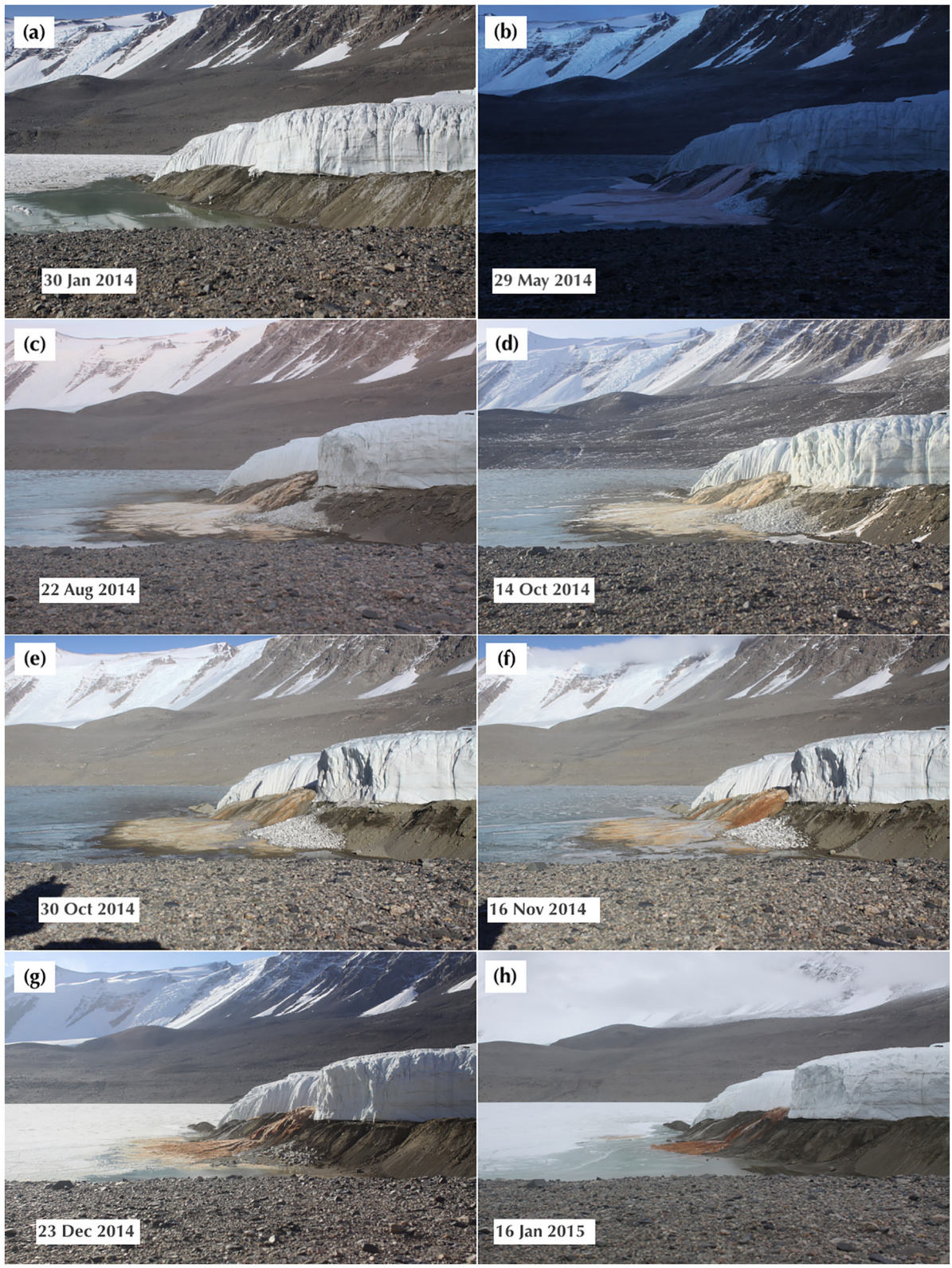

Figure 1. Time-lapse photos documenting a winter 2014 brine release event that was first visible on 13 May 2014. (a) Late summer photo prior to brine release, (b) winter photo of icing deposit after 17 days of brine discharge, (c)–(f) subsequent modification of the icing fan via melt, ablation, incision by liquids (surface meltwater and/or additional subglacially sourced brine), and (g)–(h) further modification via flooding by the lateral stream and Lake Bonney moat.

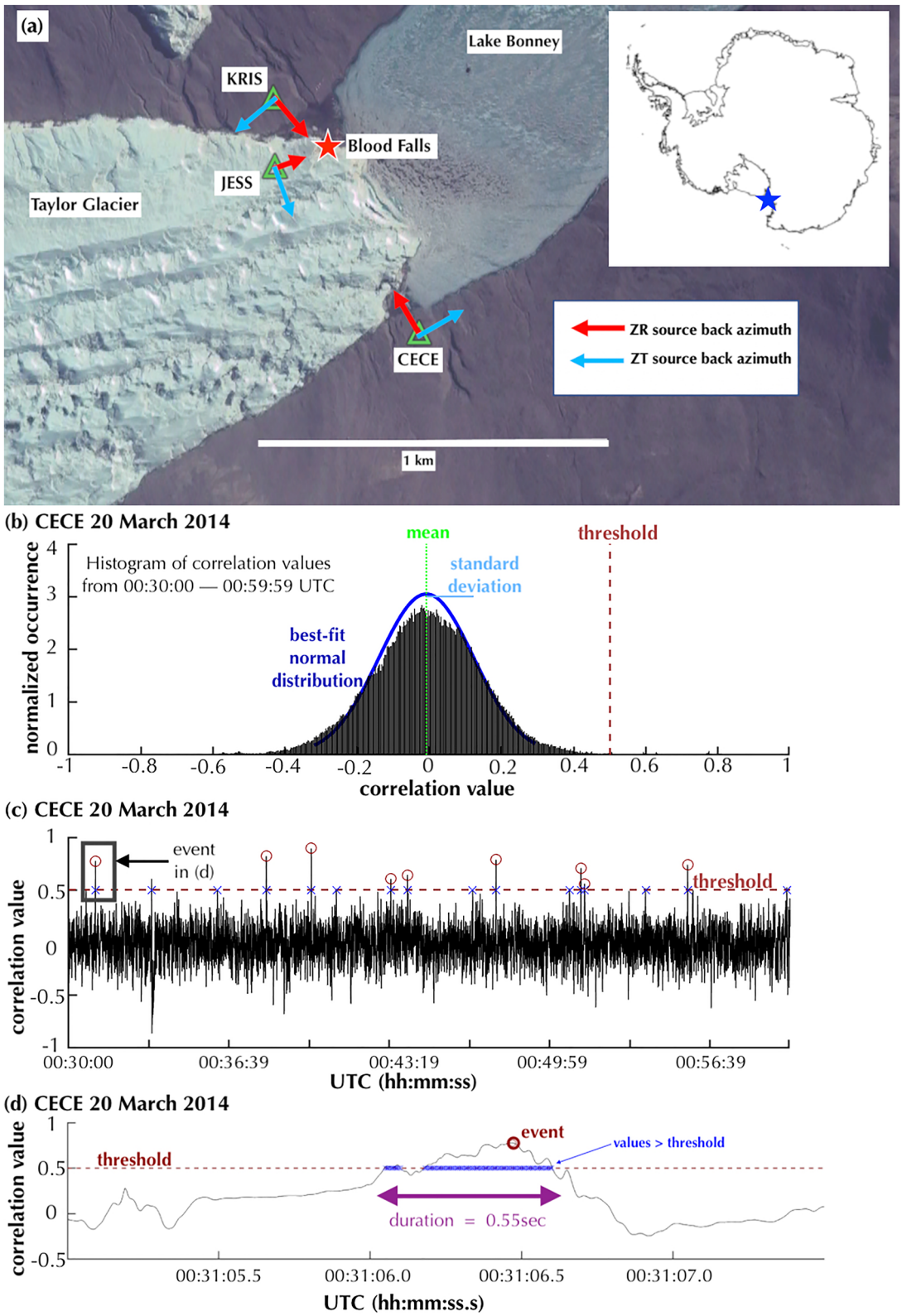
(a)
Lake Bonney
KRIS
Blood Falls
JESS
Taylor Glacier
CECE
ZR source back azimuth
ZT source back azimuth
1 km
(b) CECE 20 March 2014
Histogram of correlation values
from 00:30:00 — 00:59:59 UTC
mean
standard
deviation
threshold
best-fit
normal
distribution
normalized occurrence
correlation value
(c) CECE 20 March 2014
event
in (d)
threshold
correlation value
00:30:00
00:36:39
00:43:19
00:49:59
00:56:39
UTC (hh:mm:ss)
(d) CECE 20 March 2014
event
values > threshold
threshold
duration = 0.55sec
correlation value
00:31:05.5
00:31:06.0
00:31:06.5
00:31:07.0
UTC (hh:mm:ss.s)

Figure 2.

following the winter 2014 event also supports the idea that the subglacial brine reservoir is isolated from solar energy due to the extremely low abundance of phototropic genetic sequences (Campen et al., 2019). The geochemistry of the englacially stored brine that was sampled in situ as well as of brine discharged at the glacier surface indicates that the brine solutes represent ancient seawater that has been heavily modified through cryoconcentration and subglacial weathering (englacial brine geochemistry described by Lyons et al., 2019; geochemistry of brine sampled at the surface described by Mikucki et al., 2009).

2.2. Taylor Glacier Seismicity and Hypotheses for Brine Release Mechanisms

Seismicity at the Taylor Glacier terminus region is characterized by strong seasonal patterns. Temporally variable environmental microseismicity (seismic activity from events smaller than the threshold) is known to influence the minimum event size that short-term average to long-term average (STA/LTA) algorithms can detect (Carr et al., 2020). During the summertime, seismicity varies diurnally when surface melt is absent and seismic events are located on the glacier and lake ice (Carmichael et al., 2012). However, when surface melt occurs, the diurnal seismicity pattern is suppressed and the event size and location pattern change. Seismic activity during melt periods consists of repeating, larger events with volumetric opening source mechanisms and locations consistent with crack opening in the Blood Falls area (Carmichael et al., 2012). Therefore, meltwater-driven surface crevassing was proposed as a possible mechanism for triggering Blood Falls brine release if the surface crevasses were able to propagate deep enough (Carmichael et al., 2012).

The winter 2014 brine release we document here occurred in the absence of surface melt (see Figure 3d for temperature data from a nearby meteorological station); therefore, we do not attribute the triggering of the winter 2014 event to meltwater-driven crevassing. Nonetheless, large surface cracks were observed following the winter 2014 brine release (Figure S1 in Supporting Information S1). Similar cracks have historically been observed following brine release events at the Blood Falls site (Carr, 2021; Chapter 2). We therefore developed a Rayleigh wave activity detector to monitor the Blood Falls source region for surface waves we expect to be generated by surface crevassing (e.g., Mikesell et al., 2012).

3. Data and Methods

3.1. Time-Lapse Photos and Timestamp Correction

We deployed a time-lapse camera on the north side of the terminus with a side view of Blood Falls (Figure 1; co-located with station KRIS in Figure 2a). Intervals between photos are 2 hr except when power failure resulted in missing images. During installation, the time zone corresponding to the internal clock settings on the time-lapse camera was not recorded; we recognized this oversight during data review. Our time zone correction procedure is described in the Supporting Information (Text S1 in Supporting Information S1). The time-lapse photo data are available for public access through the U.S. Antarctic Program Data Center (Pettit, 2019).

3.2. Seismic Data and Rayleigh Wave Detector

We deployed a 3-seismometer network (Figure 2a). The network consisted of Sercel L-22 sensors (3-channel, 2 Hz sensors) that sampled surface motion at 200 Hz; power was provided by solar panel and battery assemblies. One seismometer (JESS) was installed on the glacier near Blood Falls and two (CECE, KRIS) in the frozen sediment at the lateral terminus margins. Seismometers were installed in November 2013 and removed in January 2015. Power loss at land-based station KRIS resulted in a data gap from 29 June 2014 to 1 October 2014. The other stations (CECE and JESS) recorded for the duration with no significant data gaps. We also excluded

Figure 2. (a) Seismometer locations and back azimuth directions (arrows show direction, lengths are arbitrary). ZR detections indicate a Rayleigh wave traveling in the direction from Blood Falls to the seismometer. Base image: Google, Maxar Technologies, image date: 5 December 2008. (b) Theoretical density of the ZR correlation data (blue curve) and its histogram (bars) for a 30-min window, normalized so the total area of the histogram bars equals one. The best-fit normal distribution has a mean of -8.6×10^{-3} and standard deviation of 0.13. The one-sided CFAR condition of 5×10^{-5} dictates a threshold value of 0.50. (c) Correlogram and threshold corresponding to histogram in (b); nine events (red circles) are identified above the threshold. Some correlation values exceeded the threshold (for instance: blue x's around minute 33); however, the short duration excludes these from being declared events. (d) Detail of the first event marked with box in (c). Blue x's: time indices with correlation values above the threshold. This is considered one event–the gap between the two blocks of threshold exceedances is too short to distinguish separate events. The trigger on time is 00:31:06.045 (first blue x), trigger off time is 00:31:06.595 (last blue x), the red circle indicates the event time (00:31:06.465), and correlation value detection statistic (0.7742). The event duration is 0.55 s.

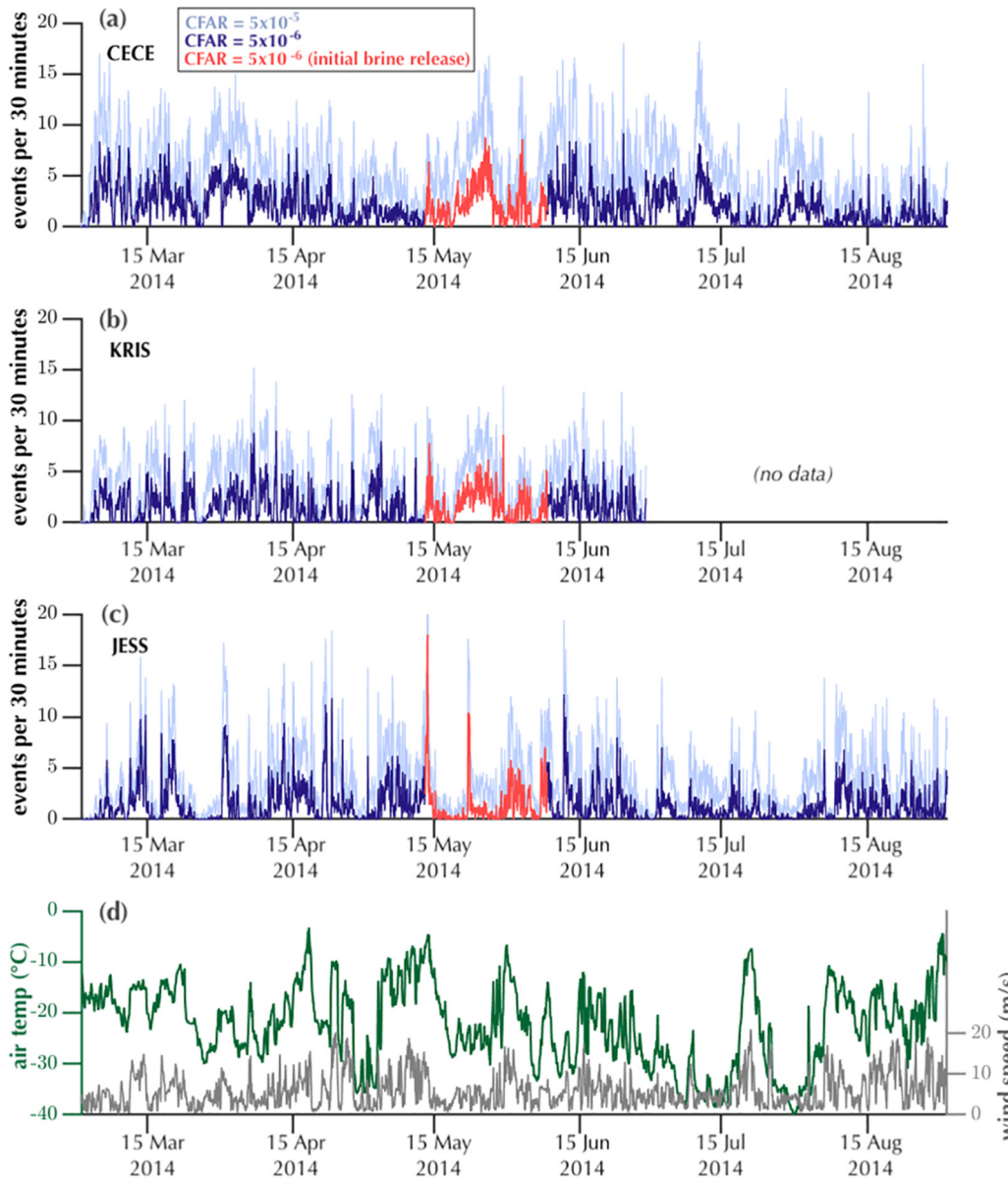

Figure 3. Events per 30 min, as identified by the Rayleigh-wave detector at (a) land-based station CECE, (b) land-based station KRIS (power failure caused data loss after June 30), and (c) on-ice station JESS (for this station, some rates above 20 events per 30 min identified using the 5×10^{-5} constant false alarm rate (CFAR) are cut off by the vertical scale, see Figure S16e in Supporting Information S1 for expanded scale). The CFAR = 5×10^{-6} condition is highlighted in dark blue and red (red indicates initial visible brine release period 13 May–8 June 2014), and the 5×10^{-5} CFAR condition results are in light blue to show the range in detected event rates. In (d), air temperature (green, left vertical axis) and wind speed (gray, right vertical axis) from the nearby Taylor Glacier meteorological station (Doran & Fountain, 2019) are plotted. All time series are smoothed with a 2 hr duration (event detection rates: 5-point, weather data: 9-point) moving window. See Figure S16 in Supporting Information S1 for time series covering the full data collection period.

portions of the data for each station based on visual review of spectrograms confirming poor data quality on one or more channels (sample spectrograms included in Figures S2–S4 in Supporting Information S1). We used the remaining data as input into our Rayleigh detector. The seismic data are available for public access through the IRIS Data Management Center (Pettit, 2013).

We use a seismic correlation detector that is based on identifying statistically significant elliptically polarized energy. Raleigh waves are characterized by deformation in the vertical and radial directions (along the radial

path from source to receiver), whereas Love waves consist of deformation in the transverse and radial directions (Stein & Wysession, 2003; p. 87–89). Rayleigh-wave detection operates on the principle that the elliptical polarized energy of a Rayleigh wave can be transformed to linearly polarized energy via a phase-shift of the vertical channel, while at the same time this transformation converts linearly polarized body waves and Love waves into elliptical polarization that do not trigger the correlation detector. Our algorithm modifies an automated Rayleigh-wave correlation detector routine described by Chael (1997). The detection of Raleigh waves from an unknown source typically requires knowing the timing of an event and scanning through possible source directions (defined as the back azimuth from the sensor) to find peak correlation values between the Hilbert-transformed vertical and rotated radial channels to infer a source location (e.g., Carmichael, 2013; Chael, 1997; Köhler et al., 2019). In contrast, we assume a known source location (Blood Falls) and monitor the correlation values through time to describe Rayleigh-wave seismicity originating along back azimuths pointing from the sensors toward Blood Falls (red arrows in Figure 2a).

Seismic detectors that test correlation statistics for the presence of seismic waveform energy are more sensitive than those that test for the presence of incoherent waveform energy, like a standard STA/LTA detector (Carmichael & Nemzek, 2019). Therefore, our detector has, in principle, the capability to identify waveforms of lower energy that originate from Blood Falls release locations compared to the STA/LTA detectors applied in our previous studies (Carr et al., 2020).

Our Rayleigh-wave detection algorithm operates as follows (Text S2 in Supporting Information S1 contains further details). For each station, we preprocess the data with detrending and bandpass filtering (passband 2.5–35 Hz) operations. We then rotate horizontal channels into a radial/transverse reference frame (methods follow Incorporated Research Institutions for Seismology, 2020) with respect to Blood Falls (Figure 2a). Next, we Hilbert transform (phase advance by $\pi/2$ radians) the vertical channel. We calculate correlation coefficients between the aligned radial and Hilbert-transformed vertical channels with a 0.75 s, tapered, sliding window. Next, we define statistically significant thresholds for detection based on best-fit probability density functions calculated for consecutive 30-min blocks of data (Figures 2b and 2c). The large-sample normality assumption for the correlation statistic is justified elsewhere (Wiechecki−Vergara et al., 2001).

To test the sensitivity of our results to our choice of threshold value, we run the algorithm with two different constant false alarm rates. A constant false alarm rate (CFAR) is defined as the probability that the detection statistic exceeds the threshold in the absence of a Rayleigh seismic event. Rayleigh events are declared when the correlation value between the radial and Hilbert-transformed vertical channel exceeds the specified threshold for at least 0.31 s. In our detector, a Rayleigh event declaration also requires a minimum temporal separation from preceding or succeeding events (3.29 s); if the temporal separation is less than this, the "events" are grouped together as a single event (see example in Figure 2d). For Rayleigh events with correlation values above the threshold, we store the event duration, maximum correlation value, and associated p-value (area under the right hand tail of the correlation distribution, with the lower integration limit defined by the detection correlation statistic). For each 30-min block, we store quantitative routine output including the parameters that shape the best-fit correlation density function, such as the mean, standard deviation, and thresholds that associate with the different CFAR conditions we implement. Examples of detected waveforms are included in Figure S5. We also calculated the dominant frequency (following methods from Douma & Snieder, 2006) and event duration of identified events as described in Text S3 and Figures S6–S8 in Supporting Information S1.

We ran the Rayleigh event detector with one-sided CFAR thresholds of 5×10^{-5} and 5×10^{-6} as a way to test the sensitivity of our results. We subjectively determined that these CFAR conditions provided the best compromise between smaller CFAR conditions wherein the detector skipped waveforms that we would have manually identified and larger CFAR conditions wherein the detector identified portions of seismograms that we could not visually attribute to Rayleigh-type signals rather than elliptically polarized background noise.

3.3. Rayleigh Detector Minimum Detectable Event Size Analysis

We perform an experiment to measure the temporal variability of the minimum event size identified by our Rayleigh detector. To do so, we estimate the minimum duration of a Rayleigh wave pulse excited by instantaneous crack formation, and then estimate both the high and low frequency limits of expected correlation between a radial and vertical channel after those waveforms are immersed in noise.

Our structural model uses physical parameters typical for cold glaciers (including seismic velocities and ice density) as well as experiment parameters specific to our 2013–2015 field seismic deployment (including the sampling interval and instrument response parameters). Specifically, we use *p*-wave and *s*-wave speeds of 3,850 m/s and 1,950 m/s for the ice layer and 4,800 m/s and 2900 m/s for the substrate half-space (values from Carmichael et al., 2012; Shean et al., 2007). We use a standard ice density of 917 kg/m^3 and a substrate density of 2700 kg/m^3 consistent with basement velocities in Taylor Valley (Table 1; Barrett & Froggatt, 1978 and references therein). The crack for the template source event is a vertical crack at the glacier surface that opens with a volumetric change of 0.01 m^3, for instance, a crack with planar surface area of 1 m by 1 m that opens 0.01 m.

Our source model is a point source with a delta source time function that excites a Rayleigh wave. A sensor located 500 m from the seismic source records the Rayleigh waveform after this waveform attenuates in ice and thereby broadens, diminishes in amplitude, and superimposes with noise. We implement a Futterman filter (Futterman, 1962) to attenuate the waveform amplitude with $Q = \sqrt{(35 * 45)}$, the geometric mean of values reported by Carmichael et al. (2015; p. 12). The Futterman filter we implement is a causal filter that uses dispersive attenuation and a physical value of Q to reproduce the effect of reducing waveform amplitude at particular frequencies (Carmichael et al., 2015; Equation 1). This attenuation broadens the peak asymmetrically so that energy cannot arrive before the propagation time from the source wavelet to the receiver (Figure 5.13; Aki & Richards, 2009). The "noise", into which we infuse the attenuated Rayleigh waveform, is a random sample of the preprocessed (detrended, filtered, and rotated) multichannel data from a specific 30-min window; this sample is cut to the same length as the synthetic source waveform.

After adding the source waveform to the noise waveform, we calculate the correlation coefficient between the radial and Hilbert-transformed vertical waveform channels. We compare this correlation value with the threshold previously determined by the Rayleigh event detector for the 30-min window the noise sample came from. If the correlation value of the template source superimposed on the noise sample does not exceed the threshold, we scale the source (scale the synthetic Rayleigh waveform) until the resulting correlation value exceeds the threshold.

We track the minimum detectable event size corresponding to the scaling required for the correlation to exceed the threshold, and repeat the experiment using thresholds and data samples from different 30-min time windows. We completed the analysis for 3 weeks during the winter (10–30 May 2014).

We used the same source model to confirm the minimum pulse width that a delta-function source would produce for experimental conditions representative of our 2013–2015 seismic installation. We used an attenuation value of 40, consistent with elsewhere in the paper. We concluded that given a 500 m source to sensor distance with a Nyquist frequency of 100 Hz, the signal from a delta-function source that attenuates and convolves with the L-22 instrument response will have a duration of 0.4 s. For the frequency band we used, this equates to about one full cycle at 2.5 Hz or about 14 full cycles at 35 Hz (see Text S4 and Figures S9–S15 in Supporting Information S1 for details).

4. Results

4.1. Wintertime Brine Outflow

During the 2014 austral winter, a time-lapse camera captured brine outflow activity as a series of pulsed events, first visible on 13 May (Figure 1) (Movie S1). Brine release continued through 8 June, after which darkness made data interpretation difficult, but outflow likely occurred through 28 June when power failure interrupted data collection (Movie S2). We refer to 13 May–8 June 2014 as the initial visible brine release period. One image was captured on 22 August, a few images were captured in mid-September, and by the end of September regular image capture restarted because solar power was available for the system to resume data collection. During the 3 weeks of initial visible brine release, air temperatures recorded at a nearby meteorological station (approximately 3 km up-glacier from Blood Falls) (Doran & Fountain, 2019) did not exceed −4.1°C and averaged −20.7°C; we therefore do not expect that any surface melt occurred.

The single image captured in August (Figure 1c) shows the fan surface had already been modified, presumably by sublimation. Subsequent, but infrequent, image collection shows that parts of the icing deposit were removed over the next several weeks. However, during October and early November, liquid is visible flowing down the icing

surface (Figures 1e and 1f). We suspect this is additional Blood Falls brine, but cannot exclude the possibility that this is meltwater from preexisting icing deposits flowing down the icing fan. Melt channels incise the fan in mid-December, and the fan is more heavily modified by melt and sublimation. By mid-January at the end of the photo record, the icing deposit is much smaller than in prior months, partly because the lateral stream and melt from the edges of Lake Bonney flood the Blood Falls fan (Figure 1h).

4.2. Rayleigh-Wave Event Detections

We plot the time series of Blood Falls back azimuth event detection rates (per 30 min) for the duration of the seismic data record in Figure S16 in Supporting information S1, and from 1 Mar to 31 Aug 2014 in Figure 3. The initial visible brine release period (13 May–8 June 2014) is highlighted in red. Gaps in the time series plots represent missing data (e.g., power failure at KRIS during July–mid-October) or when one or more channels were compromised. The North channel at CECE was not recording properly until the seismometer was serviced in late January 2014 (Figure S2 in Supporting Information S1), and all three channels at JESS failed as the 2014–2015 melt season progressed (Figure S4 in Supporting Information S1), presumably due to flooding of the installation by meltwater.

The same relative patterns of seismicity are apparent for both CFAR values. As expected, greater numbers of events are identified under the larger CFAR condition of 5×10^{-5} than 5×10^{-6} (Figure 3). We detect Rayleigh events during all times of the year, with the highest event detection rates in November–January. For part of the summertime at some stations, Rayleigh wave emission rate remains elevated (never returns to zero) for days at a time (see station JESS January 2014; Figure S16e in Supporting Information S1 and station KRIS January 2015; Figure S16c in Supporting Information S1). Typical event detection rates are on the order of 0–30 events per 30 min under the CFAR $= 5 \times 10^{-6}$ condition, but vary seasonally and by station (Figure 3 and Figure S16 in Supporting Information S1).

JESS recorded the highest 30-min event rates of the winter on 13 May 2014, at the start of the visible brine release period (tallest red peak is 18 events per 30 min in Figure 3c). Other wintertime peaks at this station are typically around 9–12 events per 30 min. From around 20–27 May 2014, during the initial visible brine release period, land-based stations CECE and KRIS (Figures 3a and 3b) recorded event rates around 2–8 events per 30 min, similar to the rest of the winter.

4.3. Detection Thresholds

We calculated the minimum event size detectable at each station for 30-min windows from 10 to 30 May 2014. In Figure 4, crack size is reported in terms of crack edge length. We first calculated the minimum event size in terms of a volumetric opening (see Section 3.3), and converted this to the equivalent linear dimensions for a crack that opens 0.01 m and has a square planar area (crack depth = crack length, we define this as "crack edge length"). Although we report our results in terms of edge length to facilitate comparison to cracks in the environment near Blood Falls, our results do not imply any specific crack aspect ratio or opening distance. The minimum detectable crack edge lengths average 2.2 and 2.3 m, respectively, for land-based stations CECE and KRIS, and 2.9 m for on-ice station JESS for a crack opening 0.01 m. The pattern of smaller thresholds for the land-based stations during the wintertime compared to the on-ice station is consistent with prior results for this data set where STA/LTA detectors were used to find events (Carr et al., 2020). For each station, there were 30-min windows for which the minimum crack edge length that would be required to declare an event was larger than the maximum crack edge length that we tested (5.6 m), so the true minimum size is unknown. These windows are marked with red x's in Figures 4a–4c.

5. Discussion

Meteorological data (Figure 3d) indicate that surface melt was not occurring during the wintertime brine outflow event. This suggests that this particular brine release was not triggered by a surface meltwater drainage event, as documented in other cold glacier settings (e.g., Boon & Sharp, 2003), and has been suggested as a potential triggering mechanism for Blood Falls brine release during the melt season (Carmichael et al., 2012). Further, our seismic analysis shows no distinct seismic signal associated with this brine release. We consider four possible

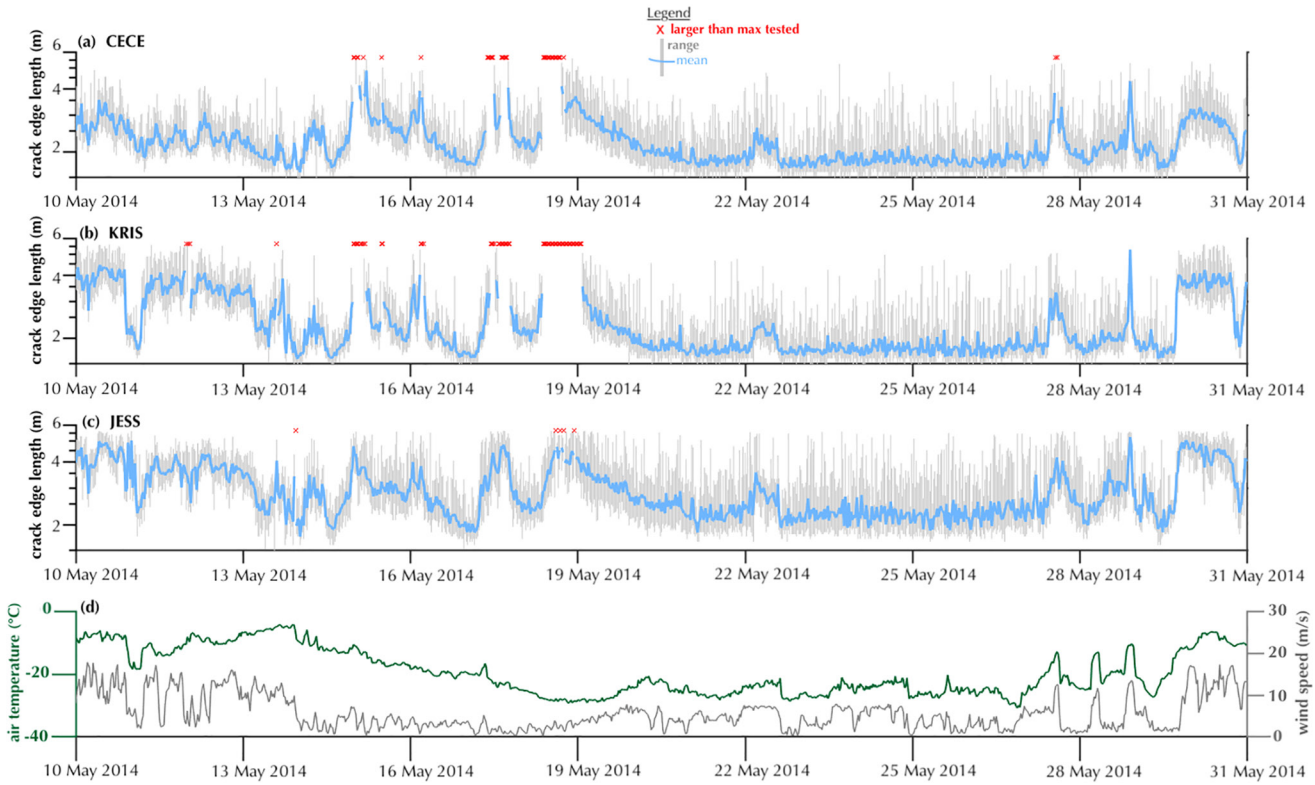

Figure 4. The smallest crack edge length (where crack edge length means the length of a side of a square planar crack that opens 0.01 m) for a Rayleigh wave-generating event that would trigger the detector at (a) CECE, (b) KRIS, and (c) JESS during 10–30 May 2014 under the 5×10^{-6} constant false alarm rate (CFAR) condition. We tested 15 different noise samples per 30-min window. For each noise sample, we determined the minimum crack size required to generate correlation values larger than the CFAR-defined threshold. The bold blue line shows the mean of the minimum crack sizes for the 15 samples and the vertical gray bars show the range of minimum detectable crack sizes. Red x's indicate 30-min windows for which the threshold crack edge length exceeds the maximum tested (5.6 m) for all noise samples (CECE: 38 windows, KRIS: 66 windows JESS: 5 windows, out of a total of 1,008, 30-min windows for each station). Note log scale of *y*-axis. (d) Air temperature (green, left vertical axis) and wind speed (gray, right vertical axis) measured at the Taylor meteorological station (Doran & Fountain, 2019). Some increases in mean minimum detectable crack edge length (particularly around 28 May 2014) appear to coincide with increases in wind speed and temperature, but the pattern is not simple.

reasons for the lack of observed seismic signature of brine release: (a) the seismic activity occurs outside of the frequency band we tested; (b) the seismic source is deeper than is detectable by our method; (c) the sources are smaller than our method can detect or aseismic; and (d) the sources are masked by myriad other environmental sources.

5.1. Hypotheses for the Apparent Lack of Brine Release Seismic Signatures

We do not observe an obvious increase in Rayleigh wave activity prior to or during brine release. A possible exception is the peak in event rate at JESS on 13 May 2014 (tallest red peak in Figure 3c), but the elevated event rate does not persist. The brief spike in event rate is not observed at the other stations. We also do not observe changes in event duration, event detection rates, or detection statistic values for Rayleigh events detected during the weeks prior to or during initial visible brine release. Instead, the dominant pattern of variation of Rayleigh-wave activity during our experiment is seasonal, with higher and more variable event detection rates during the summer. We also do not observe changes in dominant event frequency (Figure S6 in Supporting Information S1) or duration (Figure S8 in Supporting Information S1) relative to the rest of the wintertime.

5.1.1. Seismic Signature Outside the Frequency Bands of Our Experiment

The L-22 seismometers have a natural or corner frequency of 2 Hz, and for our installation the Nyquist frequency was 100 Hz (sample rate: 200 Hz). The Rayleigh detector used in this study as well as the STA/LTA detectors from our previous study (Carr et al., 2020) implement (2.5, 35) Hz bandpass filters. This filter band is

consistent with other Rayleigh-wave icequake studies (e.g., Carmichael et al., 2015; Hudson et al., 2020; Linder et al., 2019). Our Rayleigh detector imposed an effective minimum event duration of 0.31 s (see Text S2 in Supporting Information S1); we therefore cannot detect any events of shorter duration. The detector places no explicit constraint on maximum event duration (other than the theoretical limit of the 30-min window length); the maximum event durations recorded are 30–40 s, though most events last less than 10 s (Figures S7 and S8 in Supporting Information S1). Nonetheless, the frequency and duration bands we sample are similar to previously reported Rayleigh wave seismicity associated with glacier surface crevassing. Köhler et al. (2019) found Rayleigh wave events consistent with modeled source depths of <10 m to have frequencies around 1–15 Hz, with durations of <1–6 s for sources 0.8–8 km away. With a bandpass filter of (10, 80) Hz, Mikesell et al. (2012) found a dominant frequency of 45 Hz for Rayleigh wave events associated with surface crevasse opening for events located <600 m away. Carmichael (2013) similarly found Rayleigh wave events sourced by tensile surface fractures from a supraglacial lake drainage to show ∼1 s durations and 25 Hz content. We therefore expect that if there are Rayleigh-wave generating surface crevassing events at our field site, our detector should find them based on our experimental design.

At higher frequency bands than that of our experiment, researchers have identified small seismic events located deep in glaciers. For instance, Helmstetter et al. (2015) observed repeating events characterized by short duration (0.1 s), high frequency (100 Hz), impulsive arrivals and distinct body waves but no surface waves, and determined that these events represented sources deep in the glacier. The event characteristics they describe agree with seismic events that other researchers have described as basal icequakes (e.g., Dalban Canassy et al., 2013; Deichmann et al., 2000; Walter et al., 2008). The short source duration of these sources implies small physical source dimensions; Helmstetter et al. (2015) attributed the seismic signals to stick-slip motion on the order of 1 μm to 4 mm of slip. We do not expect that our detector would identify such sources for several reasons, namely the lack of surface waves and the frequency characteristics and event duration outside our experimental design. If a similar mechanism at the bed (small-scale stick-slip motion) was responsible for perturbing the connection between the subglacial brine storage and potential englacial hydrologic pathways in such a way as to trigger Blood Falls brine release, we would not expect to detect such an initiation under our experimental conditions.

5.1.2. Deep Seismic Source

The source of brittle deformation associated with the brine release could be too deep in the glacier to generate surface waves that are large enough for us to observe. Rayleigh wave displacement decays with depth from the free surface. Therefore, the absence of observed elevated surface wave energy during Blood Falls brine release could indicate that any sources of seismic energy coinciding with brine release are located deeper in the glacier. To investigate this hypothesis, we estimate the source depths that would generate Rayleigh-wave energy at our detection threshold given our experimental design (see Text S5, Figure S17, and Table S1 in Supporting Information S1). We use the radiation pattern for a crack opening in the direction of the receiver to maximize the total displacement. We refer the reader to Carmichael (2021, Equation 39) and Carr et al. (2020; Appendix C) for further documentation of the radiation pattern specific to the crack opening. We estimate that sources with depths around 2.5 km or deeper would evade detection because any Rayleigh displacement at the surface would be smaller than our detection limits. However, the glacier thickness near the terminus is much less than this estimated source depth; the glacier thickness near the terminus is tens of meters at the cliff edge, increasing to 125 m approximately 1 km up-glacier from the terminus (Badgeley et al., 2017; Pettit et al., 2014). We therefore expect that if basal crevasses excited Rayleigh wave energy, particularly in the shallow (<50 m) ice at the terminus, we would detect the events given our experimental design.

5.1.3. Events Smaller Than Detection Thresholds

Another possibility is that seismicity associated with Blood Falls release is of such a small magnitude as to be effectively aseismic at our detection levels. The expected source scale for surface crack opening, based on field observations of the Blood Falls crack (e.g., Figure S1 in Supporting Information S1) is larger than our estimated detector thresholds for surface cracks that open and excite Rayleigh wave energy within our experiment's passband (Section 4.3). However, repeated cracking with volumetric opening smaller than the detection threshold of our detector could generate the cracks we see following a brine release event while evading detection. We cannot exclude this possibility.

Along the trend direction defined by projecting the Blood Falls crack system up-glacier, an englacial zone where liquid brine partially saturates the glacial ice causes reduced electromagnetic wave velocity, observable as a scattering zone in data collected through radio echo sounding (Badgeley et al., 2017). This documented zone of heterogeneity could also attenuate seismic waves. We did not include this possible attenuation in our source model for the minimum detectable event size analysis; if we were to, we expect the threshold crack edge length to be larger for sources within this zone of partially melted brine. As described in Section 3.3, we included a homogeneous attenuation value based on values reported by Carmichael et al. (2015).

5.1.4. Masked by Environmental Microseismicity

Another hypothesis is that there is a seismic signature associated with Blood Falls brine release, but it is superimposed on background emissions such that it is not statistically significant compared to the background (non-brine release) seismicity. The relative incoherence in measured seismic emission rates between sensors (Figures 3a–3c) suggests that each receiver measures emission rates from Rayleigh wave sources that are a sum of Blood Falls and other background sources.

In the nearby environment (within a few meters to a few hundred meters of Blood Falls), there are many potential cryogenic crack sources, including cracking in the lake ice, surface cracking associated with ice cliff collapse near the terminus, and cracking of ice within the ice-cored moraines at the terminus (Figure S18 in Supporting Information S1). Our threshold detection analysis indicated that, at least for the three winter weeks we tested, the minimum crack sizes detectable at the land-based stations under the 5×10^{-6} CFAR condition have equivalent volumetric opening to cracks that are in the range of 2 m deep by 2 m long and opening 0.01 m. We know from our prior study (Carr et al., 2020) that environmental microseismicity influences STA/LTA-based event detection within this data set, and consider it highly likely that it impacts Rayleigh-wave detection as well. Next, we consider possible environmental factors that we expect to contribute to Rayleigh-wave seismicity.

5.2. Wind, Meltwater, and Thermally Driven Environmental Microseismicity

Environmental factors may both contribute to Rayleigh wave activity and impact its detection. We expect the relative importance of factors like wind and meltwater to vary on seasonal timescales. For instance, meltwater-driven fracture consistent with seismicity reported by Carmichael et al. (2012) is likely responsible for some of the observed summertime Rayleigh-wave seismicity. Surface and subsurface melt in the uppermost tens of centimeters of the glacier are seasonally limited to the summertime (Hoffman et al., 2008), when air temperatures are near or above 0°C. Our record contains evidence of diurnal seismicity characteristics during the early summer months (November and December; Figure S16 in Supporting Information S1), but as the summer progresses, the diurnal signal disappears (January; Figure S16 in Supporting Information S1). We also observed increased event rates in January that remain elevated for days (Figure S16 in Supporting Information S1). We agree with Carmichael et al. (2012) that the likely forcing factor is increased meltwater availability. The meltwater drives hydrofracture and reduces the observable seismic pattern of the early summer characterized by thermally driven diurnal cycles.

The McMurdo Dry Valleys are characterized by different wind regimes in the summer than in the winter (Obryk et al., 2020); in the winter, foehn and less frequent katabatic wind events can dramatically raise local air temperatures by up to 30°C (Nylen et al., 2004; Speirs et al., 2010). Meteorological data from the Taylor Glacier station (Doran & Fountain, 2019) during the course of our experiment is consistent with the general climatology of the Dry Valleys. In the winter, wind speeds were higher, and the largest temperature changes occurred in association with strong wind events (Figure 3d). We infer that air-temperature changes associated with these wind events can cause fracture of various ice features as described below.

Temperature changes are known to cause ice fracture through several mechanisms. Thermally induced crack formation can be sourced by thermal bending moments (MacAyeal et al., 2018), brittle fracture induced by thermal shock-sourced diffusion of heat at depth, and volumetric expansion of refreezing water at depth (Kovacs, 1992). Thermally driven fracture also occurs in frozen sediment: Rayleigh waves have been observed in association with cracking of frozen sediment during rapid temperature drops (e.g., Okkonen et al., 2020).

We suggest that year-round small seismic sources emanate from thermally induced ice and frozen sediment fracture in the glacier terminus environment. Carmichael et al. (2012) located small seismic events on the lake ice

consistent with thermal cracking. Field observations include thermally induced cracking of the ice on Lake Bonney and ice-cored moraines (Figure S18 in Supporting Information S1) and ice blisters (Figure S19 in Supporting Information S1). Ice blisters can form after a confined water body develops an ice cover if continued freezing and expansion and/or hydrostatic pressure lift part of the ice cover upward into a dome shape (Kovacs, 1992). Ice blisters have been observed on supraglacial ponds on Taylor Glacier (CGC personal observation; Figure S19 and Text S6 in Supporting Information S1), brine icing deposits in the stream at the northern margin of Taylor Glacier (Keys, 1980, Plate 8.4) and in similar hydrologic settings in nearby Dry Valleys (Chinn, 1993; Figure 6). Because of the strong connection between wind events and temperature, we expect a direct impact on thermallydriven seismicity in association with wind events, although we did not explicitly test this hypothesis.

Despite the lack of conclusive seismic signature associated with brine release events, we can propose how brine release at Blood Falls may occur. Elevated brine pressure at the bed causes basal crevassing upwards into an englacial zone. If favorably oriented surface crevasses are present, brine flow can then reach the surface. We propose that the crack opening, both of basal crevasses and expansion of pre-existing surface crevasses, consists of a series of volumetrically small opening events that do not create a seismic signature sufficient to rise above the background microseismicity.

6. Conclusions

We document a wintertime brine release at Blood Falls that began in mid-May 2014 when air temperatures were well below freezing. We do not observe an increase in Rayleigh-wave activity prior to or during onset of the 2014 winter brine release, and therefore do not find evidence for surface meltwater-driven fracture as a mechanism for brine release. The lack of evidence for meltwater-driven fracture connecting the surface to the subglacial system is consistent with brine geochemistry that indicates the brine is isolated from the supraglacial meltwater system (Lyons et al., 2019; Mikucki et al., 2009).

In our Rayleigh wave event detection experiment, we did not find convincing evidence of a diagnostic seismic signature associated with the winter 2014 brine release at Blood Falls. We consider four hypotheses for the apparent lack of elevated Rayleigh-wave activity during brine release: (a) the seismic activity is outside our experimental frequency band; (b) the seismic activity is deep enough that surface waves are not recorded; (c) the crack opening is effectively aseismic (below our detection limits); and (d) environmental seismicity not related to brine release is sufficient to mask any seismicity associated with brine release.

As we review these hypotheses and in particular, the influence that environmental microseismicity plays both in generating seismic signals and masking detection of nonenvironmental seismic signals, we cannot exclude the case that surface and/or basal crevasses occur at sizes below our detection limits. An example of how environmental microseismicity modulates event detection is the temporal variation in the size of the smallest detectable crack opening. We find that the smallest events we can detect are comparable in size to myriad cracks in the nearby glacial terminus environment (including cracks in lake ice, ice-cored moraines, ice-lidded supraglacial ponds, and the glacier surface itself). The minimum detectable event size analysis is a robust tool that can be used to characterize detector sensitivity in other noisy seismic environments.

Data Availability Statement

Time-lapse photo data are available through the U.S. Antarctic Program Data Center (Pettit, 2019) at https://www.usap-dc.org/view/dataset/601167. Seismic data (Pettit, 2013) are available through the International Federation of Digital Seismograph Networks via the IRIS Data Management Center at https://www.fdsn.org/networks/detail/YW_2013.

Acknowledgments
The U.S. National Science Foundation (NSF) Office of Polar Programs funded this work with a grant to E.C.P. (1144177). The PASSCAL Instrument Center (IRIS, NSF EAR-0552316, 1063471) provided seismic support.

References

Aki, K., & Richards, P. G. (2009). *Quantitative seismology* (2nd ed.). University Science Books.

Badgeley, J. A., Pettit, E. C., Carr, C. G., Tulaczyk, S., Mikucki, J. A., & Lyons, W. B., & MIDGE Science Team. (2017). An englacial hydrologic system of brine within a cold glacier: Blood Falls, McMurdo Dry Valleys, Antarctica. *Journal of Glaciology*, *63*(239), 387–400. https://doi.org/10.1017/jog.2017.16

Barrett, P. J., & Froggatt, P. C. (1978). Densities, porosities, and seismic velocities of some rocks from Victoria Land, Antarctica. *New Zealand Journal of Geology and Geophysics*, *21*(2), 175–187. https://doi.org/10.1080/00288306.1978.10424049

This work was conducted in cooperation with the Enceladus Explorer (EnEx) project (PI Bernd Dachwald) through grants 50NA1206 to 50NA1211 from the DLR Space Administration, and as a collaborative project with NSF grants to Jill Mikucki (1727387), Slawek Tulaczyk (1144192), and Berry Lyons (1144176). The authors thank Jessica Badgeley, Doug Bloomquist, Paul Carpenter, Susan Detweiler, Jennifer Erxleben, Tiffany Green, Jason Herbert, Cecelia Mortenson, and Thomas Nylen for their field assistance during the 2013–2014 and 2014–2015 field seasons. In addition to code written by CGC and JDC, the authors thank Kate Allstadt and Ken Creager for code development. Carl Tape, Martin Truffer, and three anonymous reviewers provided valuable feedback on this manuscript. This manuscript has been authored with number LA-UR-21-24023 by Triad National Security under Contract with the U.S. Department of Energy, Office of Defense Nuclear Nonproliferation Research and Development. The United States Government retains and the publisher, by accepting the article for publication, acknowledges that the United States Government retains a nonexclusive, paid-up, irrevocable, world-wide license to publish or reproduce the published form of this manuscript, or allow others to do so, for United States Government purposes.

Black, R. F. (1969). Saline discharges from Taylor Glacier, Victoria Land, Antarctica. *Antarctic Journal of the United States*, *4*(3), 89–90.

Black, R. F., Jackson, M. L., & Berg, T. E. (1965). Saline discharge from Taylor Glacier, Victoria Land, Antarctica. *The Journal of Geology*, *73*(1), 175–181. https://doi.org/10.1086/627053

Boon, S., & Sharp, M. (2003). The role of hydrologically-driven ice fracture in drainage system evolution on an Arctic glacier. *Geophysical Research Letters*, *30*(18), 1916. https://doi.org/10.1029/2003GL018034

Campen, R., Kowalski, J., Lyons, W. B., Tulaczyk, S., Dachwald, B., Pettit, E., et al. (2019). Microbial diversity of an Antarctic subglacial community and high-resolution replicate sampling inform hydrological connectivity in a polar desert. *Environmental Microbiology*, *21*(7), 2290–2306. https://doi.org/10.1111/1462-2920.14607

Carmichael, J. D. (2013). *Melt-triggered seismic response in hydraulically-active polar ice: Observations and methods*. (Doctoral dissertation), University of Washington. Retrieved from http://hdl.handle.net/1773/25007

Carmichael, J. D. (2021). Hypothesis tests on Rayleigh wave radiation pattern shapes: A theoretical assessment of idealized source screening. *Geophysical Journal International*, *225*(3), 1653–1671. https://doi.org/10.1093/gji/ggab055

Carmichael, J. D., Joughin, I., Behn, M. D., Das, S., King, M. A., Stevens, L., & Lizarralde, D. (2015). Seismicity on the western Greenland ice sheet: Surface fracture in the vicinity of active moulins. *Journal of Geophysical Research F: Earth Surface*, *120*(6), 1082–1106. https://doi.org/10.1002/2014JF003398

Carmichael, J. D., & Nemzek, R. J. (2019). *Uncertainty in the predictive capability of detectors that process waveforms from explosions* (p. 40). arXiv preprint Retrieved from http://arxiv.org/abs/1906.09350

Carmichael, J. D., Pettit, E. C., Hoffman, M., Fountain, A., & Hallet, B. (2012). Seismic multiplet response triggered by melt at Blood Falls, Taylor Glacier, Antarctica. *Journal of Geophysical Research*, *117*(F3), F03004. https://doi.org/10.1029/2011JF002221

Carr, C. G. (2021). *Blood Falls, Taylor Glacier, Antarctica: Subglacially-sourced outflow at the surface of a cold Polar Glacier as recorded by time-lapse photography, seismic data, and historical observations*. (Doctoral dissertation), University of Alaska Fairbanks. Retrieved from https://www.proquest.com/docview/2504856734

Carr, C. G., Carmichael, J. D., Pettit, E. C., & Truffer, M. (2020). The influence of environmental microseismicity on detection and interpretation of small-magnitude events in a polar glacier setting. *Journal of Glaciology*, *66*(259), 790–806. https://doi.org/10.1017/jog.2020.48

Chael, E. P. (1997). An automated Rayleigh-wave detection algorithm. *Bulletin of the Seismological Society of America*, *87*(1), 157–163. https://doi.org/10.1785/bssa0870010157

Chinn, T. J. (1993). Physical hydrology of the Dry Valley lakes. In W. J. Green, & E. I. Friedmann (Eds.) *Physical and Biogeographical Processes in Antarctic Lakes*, (Vol. 59, pp. 1–51). American Geophysical Union. https://doi.org/10.1029/AR059

Dalban Canassy, P., Walter, F., Husen, S., Maurer, H., Faillettaz, J., & Farinotti, D. (2013). Investigating the dynamics of an alpine glacier using probabilistic icequake locations: Triftgletscher, Switzerland. *Journal of Geophysical Research: Earth Surface*, *118*(4), 2003–2018. https://doi.org/10.1002/jgrf.20097

Deichmann, N., Ansorge, J., Scherbaum, F., Aschwanden, A., Bernardi, F., & Gudmundsson, G. H. (2000). Evidence for deep icequakes in an Alpine glacier. *Annals of Glaciology*, *31*, 85–90. https://doi.org/10.3189/172756400781820462

Doran, P. T., & Fountain, A. G. (2019). McMurdo Dry Valleys LTER: High frequency measurements from Taylor Glacier meteorological station (TARM) in Taylor Valley, Antarctica from 1994 to present. *Environmental Data Initiative*. https://doi.org/10.6073/pasta/a1df5cdab3319e9adeb18f8448fd363e

Douma, H., & Snieder, R. (2006). Correcting for bias due to noise in coda wave interferometry. *Geophysical Journal International*, *164*(1), 99–108. https://doi.org/10.1111/j.1365-246X.2005.02807.x

Elston, D. P., & Bressler, S. L. (1981). Magnetic stratigraphy of DVDP drill cores and late Cenozoic history of Taylor Valley, Transantarctic Mountains, Antarctica. In L. D. McGinnis (Ed.) *Dry Valley Drilling Project*, (Vol. 33, pp. 413–426). American Geophysical Union. https://doi.org/10.1029/AR033

Foley, N., Tulaczyk, S., Auken, E., Schamper, C., Dugan, H., Mikucki, J., & Doran, P. (2016). Helicopter-borne transient electromagnetics in high-latitude environments: An application in the McMurdo dry Valleys, Antarctica. *Geophysics*, *81*(1), WA87–WA99. https://doi.org/10.1190/geo2015-0186.1

Fountain, A. G., Tranter, M., Nylen, T. H., Lewis, K. J., & Mueller, D. R. (2004). Evolution of cryoconite holes and their contribution to meltwater runoff from glaciers in the McMurdo Dry Valleys, Antarctica. *Journal of Glaciology*, *50*(168), 35–45. https://doi.org/10.3189/172756504781830312

Futterman, W. I. (1962). Dispersive body waves. *Journal of Geophysical Research*, *67*(13), 5279–5291. https://doi.org/10.1029/JZ067i013p05279

Helmstetter, A., Nicolas, B., Comon, P., & Gay, M. (2015). Basal icequakes recorded beneath an Alpine glacier (glacier d'Argentière, Mont Blanc, France): Evidence for stick-slip motion? *Journal of Geophysical Research: Earth Surface*, *120*(3), 379–401. https://doi.org/10.1002/2014JF003288

Hodgkins, R., Tranter, M., & Dowdeswell, J. A. (2004). The characteristics and formation of a High-Arctic proglacial icing. *Geografiska Annaler Series A: Physical Geography*, *86*(3), 265–275. https://doi.org/10.1111/j.0435-3676.2004.00230.x

Hoffman, M. J., Fountain, A. G., & Liston, G. E. (2008). Surface energy balance and melt thresholds over 11 years at Taylor Glacier, Antarctica. *Journal of Geophysical Research*, *113*(F4), F04014. https://doi.org/10.1029/2008JF001029

Hudson, T. S., Brisborne, A., White, R., Kendall, J., Arthern, R., & Smith, A. (2020). Breaking the ice: Identifying hydraulically forced crevassing. *Geophysical Research Letters*, *47*, e2020GL090597. https://doi.org/10.1029/2020GL090597

Incorporated Research Institutions for Seismology (IRIS). (2020). *IRIS DMC IRISWS rotation web service documentation*. Retreived from http://service.iris.edu/irisws/rotation/1/

Irvine-Fynn, T. D. L., Hodson, A. J., Moorman, B. J., Vatne, G., & Hubbard, A. L. (2011). Polythermal glacier hydrology: A review. *Reviews of Geophysics*, *49*(4), RG4002. https://doi.org/10.1029/2010RG000350

Johnston, R. R., Fountain, A. G., & Nylen, T. H. (2005). The origin of channels on lower Taylor Glacier, McMurdo Dry Valleys, Antarctica, and their implication for water runoff. *Annals of Glaciology*, *40*, 1–7. https://doi.org/10.3189/172756405781813708

Keys, J. R. (1979). Saline discharge at the terminus of Taylor Glacier. *Antarctic Journal of the United States*, *14*(5), 82–85.

Keys, J. R. (1980). *Salts and their distribution in the McMurdo region, Antarctica* (Doctoral dissertation). Victoria University of Wellington. Retrieved from http://hdl.handle.net/10063/760

Köhler, A., Maupin, V., Nuth, C., & van Pelt, W. (2019). Characterization of seasonal glacial seismicity from a single-station on-ice record at Holtedahlfonna, Svalbard. *Annals of Glaciology*, *60*(79), 23–36. https://doi.org/10.1017/aog.2019.15

Kovacs, A. (1992). *Glacier, river and sea ice blister observations* (Tech. Rep). U.S. Army Corps of Engineers, Cold Regions Research and Engineering Laboratory.

Kowalski, J., Linder, P., Zierke, S., von Wulfen, B., Clemens, J., Konstantinidis, K., & Helbing, K. (2016). Navigation technology for exploration of glacier ice with maneuverable melting probes. *Cold Regions Science and Technology*, *123*(2), 53–70. https://doi.org/10.1016/j.coldregions.2015.11.006

Lawrence, J. P. (2017). *Evidence of subglacial brine inflow and wind-induced seiching from high temporal resolution temperature measurements in Lake Bonney, Antarctica* (Master's Thesis). Louisiana State University. Retrieved from https://digitalcommons.lsu.edu/gradschool_theses/4343

Lawrence, J. P., Doran, P. T., Winslow, L. A., & Priscu, J. C. (2020). Subglacial brine flow and wind-induced internal waves in Lake Bonney, Antarctica. *Antarctic Science*, *32*(3), 223–237. https://doi.org/10.1017/s0954102020000036

Linder, F., Laske, G., Water, F., & Doran, A. K. (2019). Crevasse-induced Rayleigh-wave azimuthal anisotropy on Glaceir de la Paine Morte, Switzerland. *Annals of Glaciology*, *60*(79), 96–111. https://doi.org/10.1017/aog.2018.25

Lyons, W. B., Mikucki, J. A., German, L. A., Welch, K. A., Welch, S. A., Gardner, C. B., & Dachwald, B. (2019). The geochemistry of englacial brine from Taylor Glacier, Antarctica. *Journal of Geophysical Research: Biogeosciences*, *124*(3), 633–648. https://doi.org/10.1029/2018JG004411

MacAyeal, D. R., Banwell, A. F., Okal, E. A., Lin, J., Willis, I. C., Goodsell, B., & MacDonald, G. J. (2018). Diurnal seismicity cycle linked to subsurface melting on an ice shelf. *Annals of Glaciology*, *60*(79), 137–157. https://doi.org/10.1017/aog.2018.29

Mikesell, T. D., van Wijk, K., Haney, M. M., Bradford, J. H., Marshall, H. P., & Harper, J. T. (2012). Monitoring glacier surface seismicity in time and space using Rayleigh waves. *Journal of Geophysical Research*, *117*(F2), 1–12. https://doi.org/10.1029/2011JF002259

Mikucki, J. A., Auken, E., Tulaczyk, S., Virginia, R. A., Schamper, C., Sørensen, K. I., & Foley, N. (2015). Deep groundwater and potential subsurface habitats beneath an Antarctic dry valley. *Nature Communications*, *6*(1), 6831. https://doi.org/10.1038/ncomms7831

Mikucki, J. A., Pearson, A., Johnston, D. T., Turchyn, A. V., Farquhar, J., Schrag, D. P., & Lee, P. A. (2009). A contemporary microbially maintained subglacial ferrous "ocean". *Science*, *324*(5925), 397–400. https://doi.org/10.1126/science.1167350

Neave, K. G., & Savage, J. C. (1970). Icequakes on the Athabasca glacier. *Journal of Geophysical Research*, *75*(8), 1351–1362. https://doi.org/10.1029/JB075i008p01351

Nylen, T. H., Fountain, A. G., & Doran, P. T. (2004). Climatology of katabatic winds in the McMurdo dry Valleys, southern Victoria Land, Antarctica. *Journal of Geophysical Research*, *109*, D03114. https://doi.org/10.1029/2003JD003937

Obryk, M. K., Doran, P. T., Fountain, A. G., Myers, M., & McKay, C. P. (2020). Climate from the McMurdo Dry Valleys, Antarctica, 1986–2017: Surface air temperature trends and redefined summer season. *Journal of Geophysical Research: Atmospheres*, *125*(13), e2019JD032180. https://doi.org/10.1029/2019JD032180

Okkonen, J., Neupauer, R. M., Kozlovskaya, E., Afonin, N., Moisio, K., Taewook, K., & Muurinen, E. (2020). Frost quakes: Crack formation by thermal stress. *Journal of Geophysical Research: Earth Surface*, *125*(9), e2020JF005616. https://doi.org/10.1029/2020JF005616

Pettit, E. C. (2013). *MIDGE: Minimally invasive direct glacial exploration of Biogeochemistry, hydrology and Glaciology of Blood Falls, McMurdo Dry Va. International Federation of Digital Seismograph Networks*. International Federation of Digital Seismograph Networks. https://doi.org/10.7914/SN/YW_2013

Pettit, E. C. (2019). *Time lapse imagery of the Blood Falls feature, Antarctica*. U.S. Antarctic Program (USAP) Data Center. https://doi.org/10.15784/601167

Pettit, E. C., Whorton, E. N., Waddington, E. D., & Sletten, R. S. (2014). Influence of debris-rich basal ice on flow of a polar glacier. *Journal of Glaciology*, *60*(223), 989–1006. https://doi.org/10.3189/2014JoG13J161

Shean, D. E., Head, J. W., III, & Marchant, D. R. (2007). Shallow seismic surveys and ice thickness estimates of the Mullins Valley debris-covered glacier, McMurdo Dry Valleys, Antarctica. *Antarctic Science*, *19*(4), 485–496. https://doi.org/10.1017/S0954102007000624

Skidmore, M. L., & Sharp, M. J. (1999). Drainage system behaviour of a High-Arctic polythermal glacier. *Annals of Glaciology*, *28*, 209–215. https://doi.org/10.3189/172756499781821922

Speirs, J. C., Steinhoff, D. F., McGowan, H. A., Bromwich, D. H., & Monaghan, A. J. (2010). Foehn winds in the McMurdo dry Valleys, Antarctica: The origin of extreme warming events. *Journal of Climate*, *23*(13), 3577–3598. https://doi.org/10.1175/2010JCLI3382.1

Stein, S., & Wysession, M. (2003). *An introduction to seismology, earthquakes, and earth structure*. Blackwell Publishing.

Walter, F., Deichmann, N., & Funk, M. (2008). Basal icequakes during changing subglacial water pressures beneath Gornergletscher, Switzerland. *Journal of Glaciology*, *54*(186), 511–521. https://doi.org/10.3189/002214308785837110

Wiechecki-Vergara, S., Gray, H. L., & Woodward, W. A. (2001). *Statistical development in support of CTBT monitoring*. Southern Methodist University.